

# Facile synthesis of homogeneous $\text{Cs}_x\text{WO}_3$ nanorods with excellent low-emissivity and NIR shielding property by a water controlled-release process†

Chongshen Guo,<sup>\*a</sup> Shu Yin,<sup>a</sup> Mei Yan<sup>b</sup> and Tsugio Sato<sup>a</sup>

Received 15th December 2010, Accepted 28th January 2011

DOI: 10.1039/c0jm04379f

A systematic investigation of the synthesis of homogenous  $\text{Cs}_x\text{WO}_3$  nanorods by a designed water-controlled release process was carried out. The results revealed that the uniform rod-like  $\text{Cs}_x\text{WO}_3$  nanoparticles with a Cs/W atomic ratio of *ca.* 0.33 can be obtained by using 20 vol%  $\text{CH}_3\text{COOH}$ –80 vol%  $\text{CH}_3\text{CH}_2\text{OH}$  mixed solution as a reaction solvent at 240 °C for 20 h. The morphology of products were changed depending on the speed of water-releasing process, meanwhile, the Cs/W atomic ratio could be controlled by both the amount of released water and the reaction temperature.  $\text{Cs}_x\text{WO}_3$  nanorods showed a high transmittance in the visible light region and excellent shielding ability of near infrared (NIR) lights, indicating that  $\text{Cs}_x\text{WO}_3$  nanorods have a suitable characteristic as solar filter applications.

## 1. Introduction

In recent years, there have been strong desires to shield the near-infrared (NIR, wavelength of 780 to 2500 nm) radiation (heat rays) by employing transparent coating on the windows of automobiles, buildings, *etc.*,<sup>1</sup> in order to reduce the energy consumption for air conditioning and thereby decrease the emission of carbon dioxide. For the application as heat rays shielding materials, an excellent shielding ability of NIR rays as well as high visible light transparency is required. In the past few years, thin films of nanosized conductive compounds such as indium tin oxides (ITOs)<sup>2</sup> and antimony-doped tin oxides (ATOs),<sup>3</sup> which were typically synthesized by using sputtering technology, were widely used as solar filters. These conductive compounds show high transparency for the visible light and a shielding ability of NIR radiations. The NIR shielding by them was considered to be caused mainly by NIR reflection. Nowadays, the NIR shielding materials with low-emissivity (low-e) are highly required.<sup>2</sup> The low-e NIR shielding materials can not only shield off the NIR lights to provide comfortable indoor environment in summer, but also act as heat-insulator to prevent radiation of heat to the outside from the room, particularly in cooling-dominated climates.

Adachi and Takeda reported that the nanoparticles of cesium tungsten ( $\text{Cs}_x\text{WO}_3$ ) with a hexagonal bronze structure (Fig. 1) showed promising performance as solar filter.<sup>4</sup> Due to the bigger size of  $\text{Cs}^+$  ion (0.17 nm), the incorporation of  $\text{Cs}^+$  into the hexagonal tunnels (0.163 nm) will induce the structure distortion of  $\text{WO}_6$  octahedral framework. Such a distortion makes the reduce-type  $\text{Cs}_x\text{WO}_3$  ( $\text{Cs}_x\text{W}_{1-x}{}^{6+}\text{W}_x{}^{5+}\text{O}_3$ ) more difficult to be controlled both in size and morphology.<sup>5</sup> Until now, most of researchers synthesized it mainly through the solid state reaction which was performed at high temperature and reductive atmosphere.<sup>6–10</sup> In a previous research we have found that the strong and typical near-infrared lights shielding properties can be realized when the particle size was smaller than 100 nm.<sup>11</sup> In this study, we developed a facile and novel solvothermal method to synthesize homogenous nanorods of tungsten bronze type  $\text{Cs}_x\text{WO}_3$  by employing a water controlled-release process

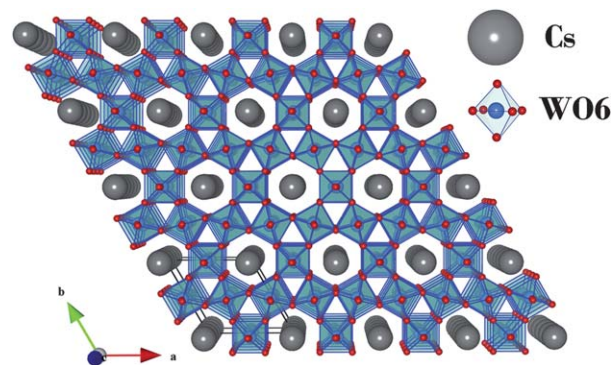


Fig. 1 Structure of  $\text{Cs}_x\text{WO}_3$  framework projected on *a*–*b* planes ( $X = 0$ –0.33).

<sup>a</sup>Institute of Multidisciplinary Research for Advanced Materials, Tohoku University, 2-1-1 Katahira, Aoba-ku, Sendai, 980-8577, Japan. E-mail: bigguop@mail.tagen.tohoku.ac.jp; Fax: +81 222175598

<sup>b</sup>Department of Chemistry, Graduate school of Science, Tohoku University, Aoba-ku, Sendai, Japan

† Electronic supplementary information (ESI) available: NMR and GC-MS analysis; AFM and SEM images; BET plots. See DOI: 10.1039/c0jm04379f

(WCRP). By precisely controlling the water releasing process based on esterification reaction between ethanol and acetate acid, monodispersed nanorods of  $\text{Cs}_x\text{WO}_3$  were produced. Such nanorods realized high transmittance in the visible light range, together with a strong absorption in the NIR light range. On the other hand, the key factors which affected the morphology and shielding performance of  $\text{Cs}_x\text{WO}_3$  nanoparticles were studied intensively. In addition, the mechanism of WCRP process and the low- $\epsilon$  performance were discussed in detail.

## 2. Experimental section

### 2.1. Materials

All the chemicals were of analytical grade and used without further purification. Tungsten hexachloride ( $\text{WCl}_6$ ), cesium hydroxide monohydrate ( $\text{CsOH}\cdot\text{H}_2\text{O}$ ), dehydrated ethanol and acetic acid anhydride were purchased from the Kanto Chemical Co. Inc. Collodion (10 wt% pyroxylin in diethyl ether and ethanol) was used as binder.

### 2.2. Synthesis

In a typical experiment, first, certain amount of  $\text{WCl}_6$  was dissolved into the dehydrated ethanol with violent stirring, then  $\text{CsOH}\cdot\text{H}_2\text{O}$  was introduced into the yellowish ethanol solution of  $\text{WCl}_6$ . After the mixture became homogeneous, 0–20 ml acetic acid was introduced into the solution. The total volume of acetic acid and ethanol mixed solvent was 50 ml. The final concentration of  $\text{WCl}_6$  was adjusted to 0.015 M and nominal Cs/W atomic ratio was 0.5. After that the solutions were transferred into a Teflon-lined autoclave of 100 ml internal volume, followed by solvothermal reactions in an electric oven at 140–240 °C for 20 h. After the reaction, the dark blue products were centrifuged, washed with water and ethanol 4 times and finally dried in vacuum at 60 °C. In order to evaluate NIR shielding characteristics,  $\text{Cs}_x\text{WO}_3$  powder was dispersed in collodion–ethanol mixed solution at a mass ratio of ethanol : collodion :  $\text{Cs}_x\text{WO}_3$  = 1.0 : 0.93 : 0.15. Then, the coating solution was painted on a quartz glass by an applicator with a concave in depth of 12.5  $\mu\text{m}$ .

### 2.3. Characterization

The phase compositions of the samples were determined by X-ray diffraction analysis (XRD, Shimadzu XD-1) using graphite-monochromized  $\text{CuK}\alpha$  radiation. The size and shape of the nanoparticles were observed by transmission electron microscopy (TEM, JEOLJEM-2010). HRTEM images and SAED images were obtained on ZEISS LEO 922 with an accelerating voltage of 200 kV. The particle distribution was analyzed by a laser diffraction particle size analyzer (Shimadzu SALD-7000), providing number-based mean particle size. The optical response of the coating was measured by using a spectrophotometer (JASCO V-670), giving output of transmittance in the UV, visible, and infrared ranges (200–2700 nm). Energy-dispersive X-ray spectrometer (EDS) was employed for approximate elemental analyses. The surface composition of the samples and binding energy of  $\text{W}_{4f}$  were determined by X-ray photoelectron spectroscopy (XPS, Perkin Elmer PHI 5600).  $^1\text{H}$  NMR spectra

were recorded on a JEOL JMTC-270/54/SS (JASTEC, 300 MHz) spectrometer. The specific surface area of a sample was measured by a surface area and pore size analyzer (Quanta Chrome Instruments, Nova 4200-e).

## 3. Results and discussion

### 3.1. Influence of the acetic acid content

Fig. 2 shows the X-ray diffraction (XRD) patterns of the as-synthesized  $\text{Cs}_x\text{WO}_3$  particles obtained in pure ethanol and ethanol–acetic acid mixed solution containing different amounts of acetic acid at 240 °C for 20 h. All peaks could be indexed to the hexagonal cesium tungsten bronze (JCPDS No. 831334) and no impurity peak was identified. It can be seen that the sample obtained in pure ethanol (Fig. 2(a)) showed sharper peaks, indicating its larger particle size than those obtained in ethanol–acetic acid mixed solution. It was reported that the aspect ratio of the nanostructures of gold and silver could be related to the difference between the intensities of specific reflections in the XRD pattern. However, such a phenomenon was not observed in this work.

The particle size distribution profiles of the  $\text{Cs}_x\text{WO}_3$  particles synthesized in pure ethanol and ethanol–acetic acid mixed solutions with different acetic acid concentrations are shown in Fig. 3. The particles obtained in the pure ethanol showed polydispersity in particle size and relatively larger particle size with an average particle size of 1359 nm ( $d_{50}$ ) (Fig. 3(a)). In contrast, all the samples formed in ethanol–acetic acid mixed solutions with an acetic acid content of 10–40 vol% showed homogenous and narrow particle size distributions of 60–100 nm (Fig. 3(b)–(d)),

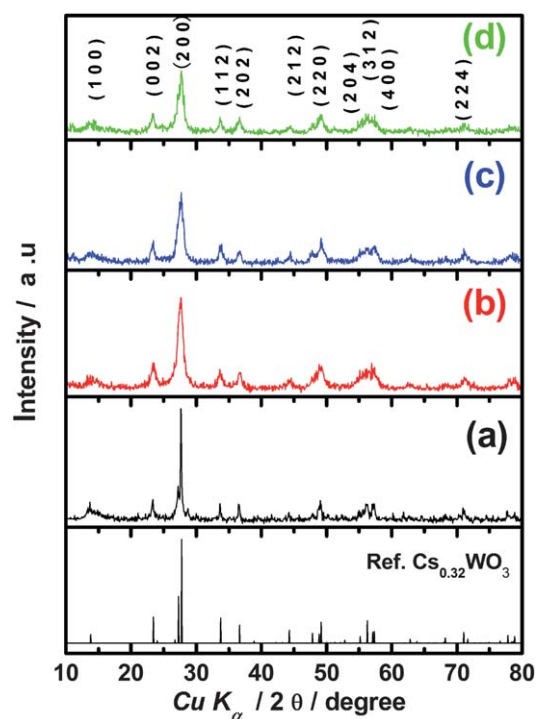
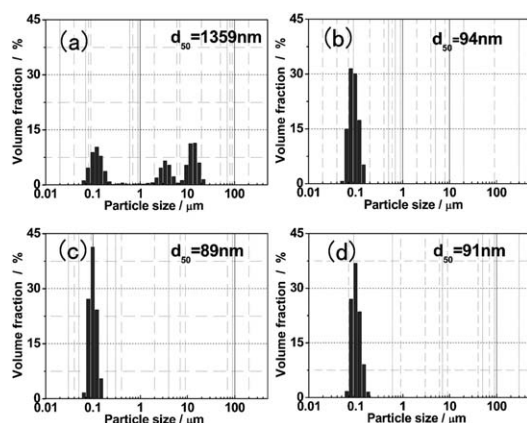


Fig. 2 XRD patterns of  $\text{Cs}_x\text{WO}_3$  particles synthesized in (a) pure ethanol and ethanol–acetic acid mixed solutions containing (b) 10 vol% (c) 20 vol% and (d) 40 vol% acetic acid at 240 °C for 20 h with a nominal Cs/W atomic ratio of 0.5 (reference:  $\text{Cs}_{0.32}\text{WO}_3$ , JCPDS No. 831334).



**Fig. 3** Particle size distributions of  $\text{Cs}_x\text{WO}_3$  particles synthesized in (a) pure ethanol and ethanol–acetic acid mixed solutions containing (b) 10 vol%, (c) 20 vol% and (d) 40 vol% acetic acid at 240 °C for 20 h with a nominal Cs/W atomic ratio of 0.5.

indicating that the acetic acid ion adsorbed on the surface of  $\text{Cs}_x\text{WO}_3$  particles played an important role to reduce the degree of particle agglomeration by the interfacial electric repulsion force. These results agreed well with the XRD profiles of the samples shown in Fig. 2.

Fig. 4 shows the typical TEM images of as-prepared  $\text{Cs}_x\text{WO}_3$  particles synthesized in pure ethanol and ethanol–acetic acid mixed solvents. It can be seen that the irregularly agglomerated larger particles were formed in pure ethanol (Fig. 4(a)). In contrast, the samples synthesized in 10 vol% and 20 vol% acetic acid contained ethanol solution consisted of rod-like nanosized particles with *ca.* 15 nm in diameter and 50 nm in length (Fig. 4(b) and (c)). The aspect ratio, which is defined by the ratio of maximum Feret diameter to minimum Feret diameter, was calculated as 4–6 for nanorods. By increasing the acetic acid concentration to 40 vol%, the size of  $\text{Cs}_x\text{WO}_3$  nanorods could be decreased, but the particle agglomeration tended to proceed a little (Fig. 4(d)). The BET specific surface areas of samples

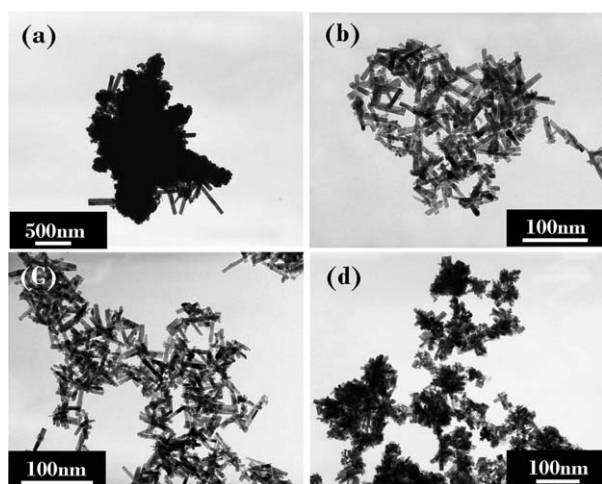


**Fig. 4** TEM images of  $\text{Cs}_x\text{WO}_3$  particles synthesized in (a) pure ethanol and ethanol–acetic acid mixed solutions containing (b) 10 vol%, (c) 20 vol% and (d) 40 vol% acetic acid at 240 °C for 20 h with a nominal Cs/W atomic ratio of 0.5.

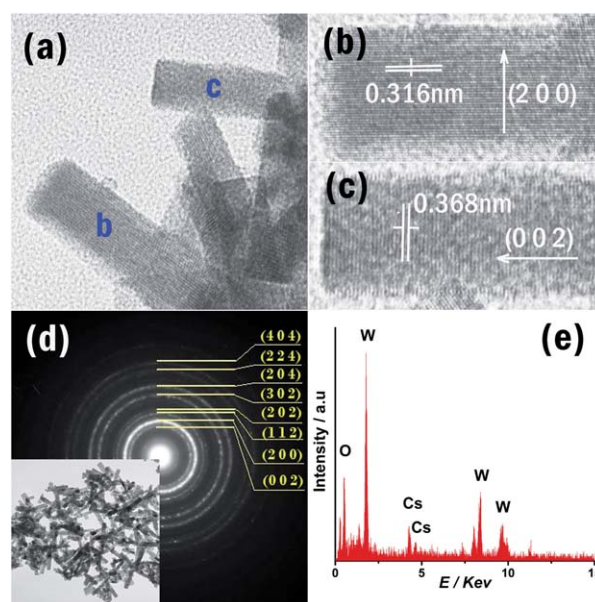


**Fig. 5** (a)–(c) HR-TEM images of selected area, (d) SAED pattern (inset shows the diffraction area) and (e) EDS pattern of  $\text{Cs}_x\text{WO}_3$  nanorods prepared in 80 vol% ethanol–20 vol% acetic acid mixed solution at 240 °C for 20 h with a nominal Cs/W atomic ratio of 0.5.

a–d determined by  $\text{N}_2$  adsorption were 11.7, 67.3, 77.7 and 65.3  $\text{m}^2 \text{g}^{-1}$ , respectively (see also Fig. S3†).

Fig. 5 shows the HR-TEM, ED and EDS patterns of  $\text{Cs}_x\text{WO}_3$  nanorods as-synthesized in 80 vol% ethanol–20 vol% acetic acid mixed solution. The  $\text{Cs}_x\text{WO}_3$  with one-dimensional hexagonal channel structure of tungsten bronze (Fig. 1) is preferential to grow along the *C*-axis and this supposition could be confirmed by the HR-TEM images (Fig. 5(a)–(c)). The crystalline lattice constants in the direction of parallel and perpendicular to the nanorod were calculated as 0.368 nm and 0.316 nm, respectively, and were identified as the crystal panel of (0 0 2) and (2 0 0), respectively. The chemical composition analysis based on the EDS (Fig. 5(d)) indicated the existence of Cs and W elements.

In order to confirm the formation mechanism of the cesium tungsten bronze under present reaction conditions, the components of the mother liquids after reactions in ethanol and ethanol–acetic acid mixed solutions were analyzed by NMR and GC-MS (Fig. S1, S2 and Table S1†). It was found that when pure ethanol was used as a solvent, diethyl ether was formed during the reaction in ethanol, while diethyl ether and ethyl acetate were formed when reaction was conducted in ethanol–acetic acid mixed solution. These results suggested that when pure ethanol was used as a reaction solvent, the dehydration condensation reaction of ethanol to form diethyl ether and water was occurred as shown by eqn (1).



On the other hand, when the ethanol–acetic acid mixed solution was utilized, the esterification reaction to form ethyl acetate and water as shown in eqn (2) also occurred together with the dehydration condensation reaction of ethanol (eqn (1)).



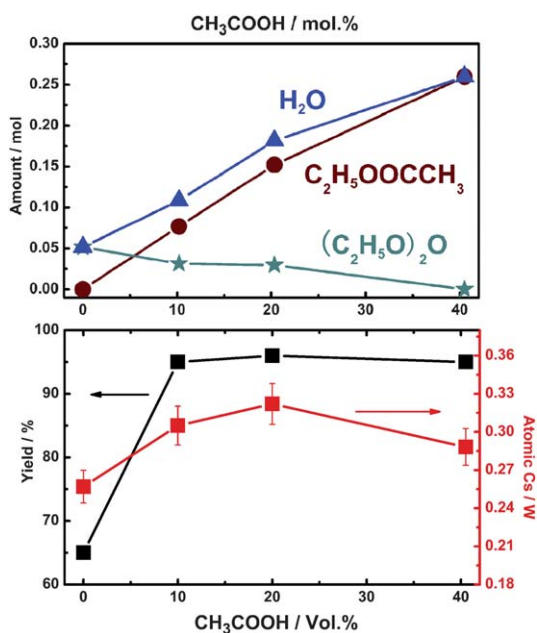
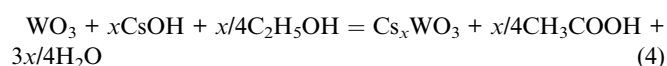
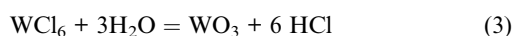


**Fig. 6** Amounts of acetyl acetate, diethyl ether and water, Cs/W atomic ratio in  $\text{Cs}_x\text{WO}_3$  and  $\text{Cs}_x\text{WO}_3$  yield as a function of acetic acid content in ethanol at 240 °C for 20 h with a Cs/W atomic ratio of 0.5.

The amounts of acetyl acetate and diethyl ether and water, Cs/W atomic ratio in  $\text{Cs}_x\text{WO}_3$  determined by an energy-dispersive X-ray spectrometer (EDS) analysis and  $\text{Cs}_x\text{WO}_3$  yield are shown in Fig. 6 as a function of acetic acid content, where the amount of water was calculated as the total of ethyl acetate and diethyl ether according to the eqn (1) and (2). It can be seen that the amount of ethyl acetate and water increased with an increase in acetic acid content, while that of diethyl ether was decreased. Although eqn (1) and (2) released water with the same stoichiometry, the tendency of them was quite different. The etherification reaction (2) was easier to be taken place than that of reaction (1). It is reasonable to suggest that the addition of acetic acid promotes the formation of ethyl acetate and depresses that of diethyl ether, since the esterification and dehydration condensation reactions shown by eqn (1) and (2) are the equilibrium reactions. It is notable that the  $\text{Cs}_x\text{WO}_3$  yield was greatly increased with an increase in the amount of water formed by the addition of acetic acid in ethanol. This indicated that water generated by the reactions (1) and (2) as well as ethanol might play an important role to form  $\text{Cs}_x\text{WO}_3$  nanoparticles, *i.e.*, water promotes the hydrolysis of  $\text{WCl}_6$  and ethanol promotes the reduction of  $\text{W}^{6+}$  to  $\text{W}^{5+}$  to form  $\text{Cs}_x\text{WO}_3$  as shown by eqn (3) and (4). In addition, acetic acid acts to depress the agglomeration of particles by the electrostatic repulsion force by forming negatively charged particles. It is reasonable to suggest that the  $\text{WO}_3$  was a short-lived reaction intermediate and reacted further to  $\text{Cs}_x\text{WO}_3$  as soon as it is formed.



The atomic ratio of Cs/W in  $\text{Cs}_x\text{WO}_3$  increased at first from 0.26 to 0.32 with an increase in acetic acid content from 0 to 20

vol%, and then decreased to 0.29 at 40 vol%. It is notable that well dispersed nanorods of  $\text{Cs}_x\text{WO}_3$  with the Cs/W atomic ratio of almost 0.33 which is the ideal value of tungsten bronze structure were directly produced by the facile solvothermal reaction in 80 vol% ethanol–20 vol% acetic acid mixed solution. Based on above results, it might be suggested that the water controlled-release process is useful to fabricate the homogenous  $\text{Cs}_{0.33}\text{WO}_3$  nanorods. In other words, the insertion amount of  $\text{Cs}^+$  into the  $\text{WO}_3$  crystal is determined by the amount of released water, *i.e.*, when the amount of water is few, the formation of  $\text{Cs}_x\text{WO}_3$  does not proceed effectively and  $\text{Cs}_x\text{WO}_3$  with low Cs/W atomic ratio is formed with low yield. On the other hand, in the presence of excess amount of water, Cs/W atomic ratio decreases due to the elution of  $\text{Cs}^+$  in the solution by the ion exchange reaction shown by eqn (5).



In our experimental conditions, the amount of acetic acid was much more than that of  $\text{OH}^-$  originated from eqn (5). Therefore, the deprotonation of acetic acid was negligible.

The formation mechanism of  $\text{Cs}_x\text{WO}_3$  nanorods by WCRP process can be explained as follows: for fabrication of homogenous nanorods, appropriate reaction rate and quantity of water generation are required. In the case of pure ethanol solvent, due to the low reaction rate of the dehydration condensation reaction of ethanol to generate water, the rate of  $\text{Cs}_x\text{WO}_3$  formation *via* reactions (3) and (4) is slow, therefore, small amounts of nuclei are formed to generate large particles of  $\text{Cs}_x\text{WO}_3$  (Fig.4(a)). By adding acetic acid in ethanol, since the rate of water generation increases, the amount of crystal nuclei increases to decrease the particle size of  $\text{Cs}_x\text{WO}_3$ . In addition, acetate ion adsorbed on the surface of the  $\text{Cs}_x\text{WO}_3$  may play an important role to avoid the particle agglomeration by the electrostatic repulsion force and such capping process also facilitated the  $\text{Cs}_x\text{WO}_3$  to grow along one-direction. However, when excess amount of acetic acid is added in ethanol, the water-releasing rate becomes too high to result in the formation of aggregated non-homogeneous  $\text{Cs}_x\text{WO}_3$  particles with low Cs/W atomic ratio (Fig. 4(d)). Therefore, the optimum acetic acid content exists to form well dispersed nanoparticles of  $\text{Cs}_{0.33}\text{WO}_3$  by the WCRP process in ethanol–acetic acid mixed solutions.

The typical X-ray photoelectron spectrum of the core level tungsten ( $\text{W}_{4f}$ ) of (a) as-synthesized  $\text{Cs}_x\text{WO}_3$  nanorods is shown in Fig. 7 together with those of (b)  $\text{WO}_{2.72}$  and (c)  $\text{WO}_3$  for comparison. The curves can be fitted as two spin-orbit doublets,  $\text{W}_{4f_{7/2}}$  and  $\text{W}_{4f_{5/2}}$  for the interval of about 2.1 eV. The peaks at 34.6 and 36.7 eV, and 35.8 and 37.9 eV were attributed to  $\text{W}^{5+}$  and  $\text{W}^{6+}$ , respectively, which agreed with the reported values.<sup>12,13</sup>

Tungsten trioxide ( $\text{WO}_3$ ) possessed a wide band gap of 2.62 eV and was transparent in visible and NIR light range (Fig. 8(a)). Fig. 8(b)–(e) shows the transmittance spectra of  $\text{Cs}_x\text{WO}_3$  synthesized in various ethanol–acetic acid mixed solutions. The sample synthesized in pure ethanol showed lower visible light transparency and NIR shielding performance than those synthesized in ethanol–acetic acid mixed solutions mainly due to its irregular large particles and low Cs/W atomic ratio (Fig. 8(b)). It can be seen that the sample synthesized in ethanol–acetic acid mixed solution with 40 vol% acetic acid showed high

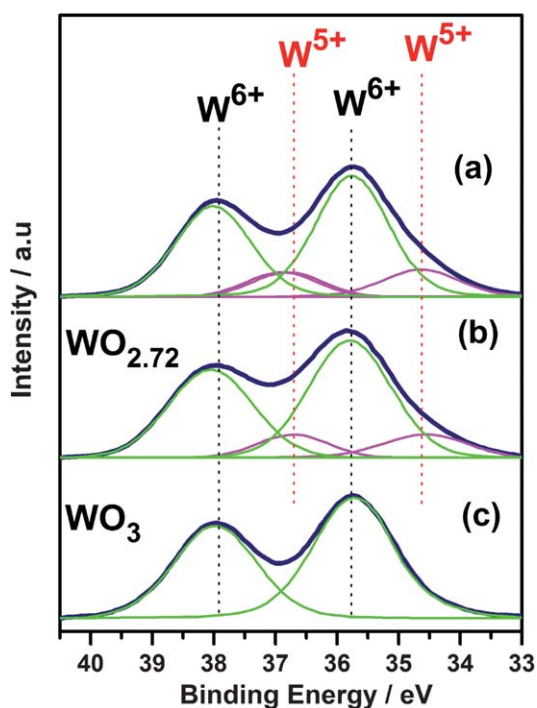


**Fig. 7**  $W_{4f}$  core-level XPS spectra of (a)  $Cs_xWO_3$  nanorods prepared in 80 vol% ethanol–20 vol% acetic acid mixed solution at 240 °C for 20 h with Cs/W atomic ratio of 0.5, (b)  $WO_{2.72}$  and (c)  $WO_3$ .

transmittance of visible light, but the NIR shielding performance was modest (Fig. 8(c)). In contrast, the samples synthesized in ethanol–acetic acid mixed solutions with 10 and 20 vol% acetic acid showed high transmittance in visible region as well as excellence shielding properties in the NIR region (Fig. 8(d) and (e)). Since the samples synthesized in ethanol–acetic acid mixed solutions of 10–20 vol% acetic acid consisted of similar size of rod-like nanoparticles, the NIR shielding performance seemed to be improved with increasing Cs/W atomic ratio and the dispersibility of  $Cs_xWO_3$  particles.

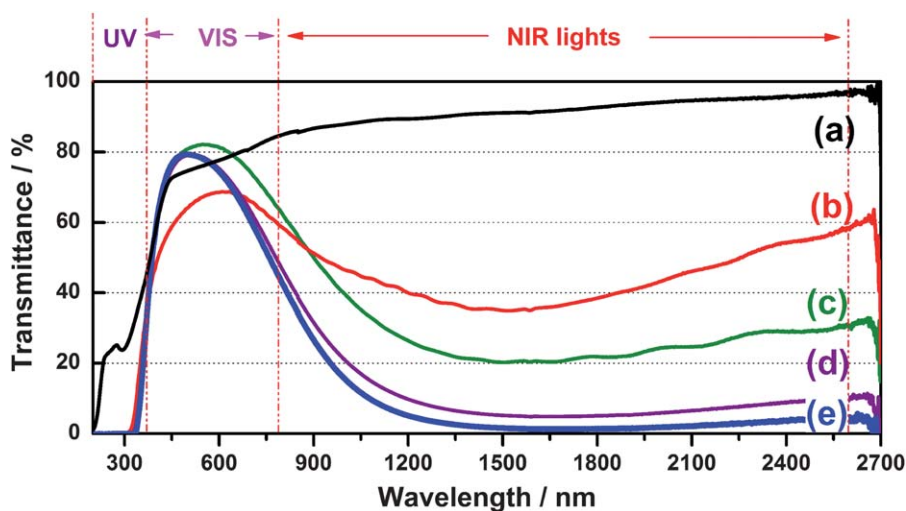


**Fig. 8** Transmittance spectra of (a)  $WO_3$ ,  $Cs_xWO_3$  particles synthesized in (b) pure ethanol, (c) 60 vol% ethanol–40 vol% acetic acid, (d) 90 vol% ethanol–10 vol% acetic acid, and (e) 80 vol% ethanol–20 vol% acetic acid solutions at 240 °C for 20 h with Cs/W atomic ratio of 0.5.

There are several key parameters which influence the performance of  $Cs_xWO_3$  solar filters. Firstly, it is accepted that the visible light transparency can be increased by decreasing particle size because of the decrease in the scattering of visible light. Adachi<sup>14,15</sup> found that the characteristic extinction in NIR region can be realized when the particle size was reduced below certain region. Secondly, the amount of  $Cs^+$  incorporated in  $Cs_xWO_3$  also strongly affects the NIR shielding properties. Each Cs ion contributes one electron to the tungsten conduction band,<sup>16,17</sup> and the origin of the shielding performance in  $Cs_xWO_3$  was closely related to the number of free electrons as discussed in a previous work.<sup>4</sup> Finally, morphology-determined optical effects may also affect the NIR shielding property.

The excellent NIR absorption property of rod-like  $Cs_xWO_3$  bronze synthesized by WCRSP process might be related to its homogeneous rod-like morphology, small particle size and high Cs/W ratio.<sup>11</sup>

### 3.2. Effect of reaction temperature

In order to investigate the influence of reaction temperature on the optical performance of  $Cs_xWO_3$  bronze, the water controlled release process was carried out at various temperatures by employing 80 vol% ethanol–20 vol% acetic acid mixed solution as a reaction solvent. UV-Vis-NIR transmittance spectra of the thin films of the products are shown in Fig. 9 together with the Cs/W atomic ratio (Fig. 9, inset). All samples prepared under present conditions consisted of similar size of rod-like nanoparticles, but the Cs/W atomic ratio increased from 0.22 to 0.32 with an increase in the reaction temperature from 140 to 240 °C. It was suggested that the effective capping process together with slow water-release process prohibit particles to grow bigger regardless of temperature change under our experimental conditions. The NIR shielding performance also increased with an increase in the reaction temperature, while the transparency in visible light region was almost the same. These results also suggested that it is important to increase the Cs/W ratio close to 0.33

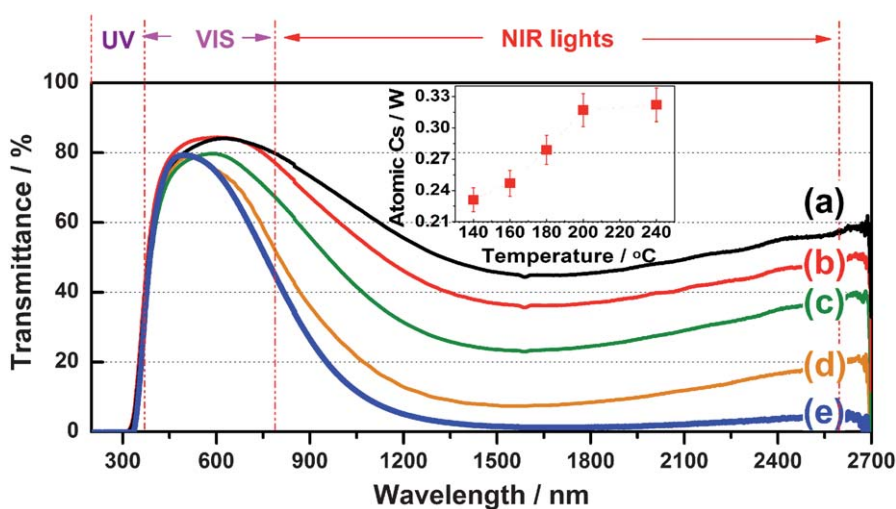


**Fig. 9** Transmittance spectra of  $\text{Cs}_x\text{WO}_3$  particles synthesized in 80 vol% ethanol–20 vol% acetic acid mixed solution at (a) 140 °C, (b) 160 °C, (c) 180 °C, (d) 200 °C and (e) 240 °C for 20 h with Cs/W atomic ratio of 0.5.

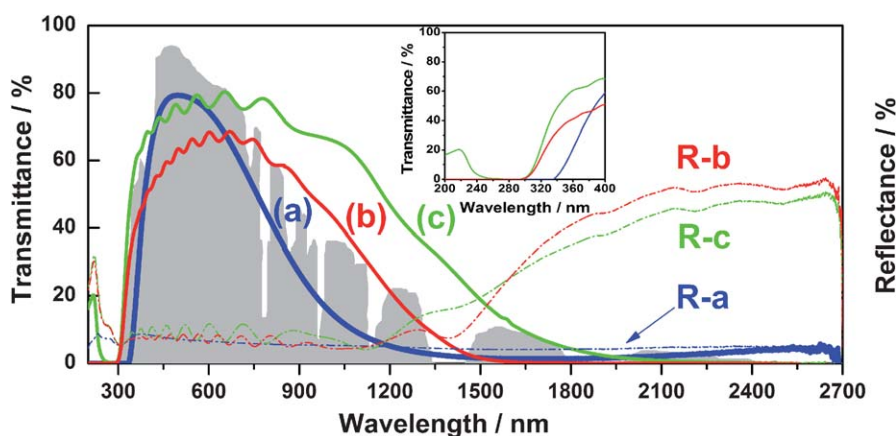


**Fig. 10** Transmittance (a, b, c) and reflectance (R-a, R-b, R-c) spectra of (a)  $\text{Cs}_x\text{WO}_3$  nanorods synthesized by WCRP process; (b) ITO glass ( $5 \Omega \square^{-1}$ ); and (c) ITO glass ( $10 \Omega \square^{-1}$ ). The background shows the relative energy wavelength distribution of solar spectrum on the sea level.<sup>18</sup>

of the ideal value in order to improve the NIR shielding performance.

### 3.3. Low-emissivity properties of $\text{Cs}_x\text{WO}_3$ nanorods

Fig. 10 shows the transmittance and reflectance profiles of  $\text{Cs}_x\text{WO}_3$  nanorods prepared by the water controlled-release process together with those of commercial ITO glasses. The ITO glasses are widely used and well-known as effective infrared-ray cutoff material.<sup>19–21</sup> When the maximum transmittance in the visible region was adjusted nearly the same as those of ITO glasses, it is obvious that the  $\text{Cs}_x\text{WO}_3$  synthesized from the novel water controlled-release process showed superior performance to ITO glass of  $10 \Omega \square^{-1}$  (Fig. 10(c)), due to its stronger absorption properties both in NIR region and UV region (enlarged area). In the case of employing ITO glass with low electric resistance of  $5 \Omega \square^{-1}$  (Fig. 10(b)), although the blue shift of NIR absorption wavelength was observed, the NIR absorption ability in the short-wavelength region around 800–1200 nm was still not

enough. In addition, it showed lower transmittance of visible light.

The value of  $100 - T(\%)$  should be the sum of absorption ( $A\%$ ) and reflectance ( $R\%$ ) of light, where  $T(\%)$  is transmittance. It can be seen that the reflectance of  $\text{Cs}_x\text{WO}_3$  sample (R-a) was quite limited in all wavelengths range, indicating the shielding of NIR light by  $\text{Cs}_x\text{WO}_3$  was mainly caused by the absorption of light. In contrast, ITO glasses showed strong light reflectance ( $R\%$ ) in the NIR region, indicating that the NIR shielding by ITO glasses is mostly caused by the reflectance instead of absorption of light.

## 4. Conclusions

Synthesis of homogenous  $\text{Cs}_x\text{WO}_3$  nanorods by a designed water-controlled release process has been investigated systematically as a function of volume percentages of acetic acid and reaction temperature. Rod-like  $\text{Cs}_x\text{WO}_3$  nanoparticles could be produced by employing 10–20 vol% acetic acid contained ethanol as a reaction solvent and the maximum Cs/W atomic ratio of *ca.* 0.33 was realized when  $\text{Cs}_x\text{WO}_3$  synthesized in

80 vol% ethanol–20 vol% acetic acid mixed solvent at 240 °C. The nanorods of  $\text{Cs}_x\text{WO}_3$  prepared by the water controlled-release process showed a pronounced absorption of NIR lights and excellent visible light transmittance. Due to low reflectance of lights, the  $\text{Cs}_x\text{WO}_3$  nanorods thin film shield off the NIR radiations mainly by absorption. This original and novel WCRP method may possess great potential for the fabrication of various kinds of functional nanoparticles.

## Acknowledgements

This research was supported in part by the Management Expenses Grants for National Universities Corporations from the Ministry of Education, Culture, Sports, Science for Technology of Japan (MEXT), and by the Adaptable and Seamless Technology transfer Program through target-driven R&D, JST, and Grant-in-Aid for Science Research (No. 20360293 & No. 22651022).

## References

- 1 I. Hamberg and C. G. Granqvist, *J. Appl. Phys.*, 1986, **60**, R123–R159.
- 2 M. Okada, Y. Yamada, P. Jin, M. Tazawa and K. Yoshimura, *Thin Solid Films*, 2003, **442**, 217–221.
- 3 E. Elangovan, S. A. Shivashankar and K. Ramamurthi, *J. Cryst. Growth*, 2005, **276**, 215–221.
- 4 H. Takeda and K. Adachi, *J. Am. Ceram. Soc.*, 2007, **90**, 4059–4061.
- 5 J. X. Liu, Y. Ando, X. L. Dong, F. Shi, S. Yin, K. Adachi, T. Chonan, A. Tanaka and T. Sato, *J. Solid State Chem.*, 2010, **183**, 2456–2460.
- 6 K. S. Lee, D. K. Seo and M. H. Whangbo, *J. Am. Chem. Soc.*, 1997, **119**, 4043–4049.
- 7 E. O. Brimm, J. C. Brantley, J. H. Lorenz and M. H. Jellinek, *J. Am. Chem. Soc.*, 1951, **73**, 5427–5432.
- 8 B. Brown and W. E. Banks, *J. Am. Chem. Soc.*, 1954, **76**, 963–966.
- 9 S. V. Vakarín, A. N. Baraboshkin, K. A. Kaliev and V. G. Zyrianov, *J. Cryst. Growth*, 1995, **151**, 121–126.
- 10 C. Kasla and M. J. R. Hoch, *J. Appl. Phys.*, 2006, **99**, 063711–063716.
- 11 C. S. Guo, S. Yin, P. L. Zhang, M. Yan, K. Adachi, T. Chonan and T. Sato, *J. Mater. Chem.*, 2010, **20**, 8227–8229.
- 12 Z. J. Gu, Y. Ma, T. Y. Zhai, B. Gao, W. S. Yang and J. N. Yao, *Chem.–Eur. J.*, 2006, **12**, 7717–7723.
- 13 D. G. Barton, M. Shtein, R. D. Wilson, D. G. Barton, M. Shtein, R. D. Wilson, S. L. Soled and E. Iglesia, *J. Phys. Chem. B*, 1999, **103**, 630–640.
- 14 K. Adachi and M. Miratsu, *J. Mater. Res.*, 2010, **25**, 510–521.
- 15 H. Takeda, H. Kuno and K. Adachi, *J. Am. Ceram. Soc.*, 2008, **91**, 2897–2902.
- 16 M. R. Skokan, W. G. Moulton and R. C. Morris, *Phys. Rev. B: Condens. Matter Mater. Phys.*, 1979, **20**, 3670–3677.
- 17 W. R. Gardner and G. C. Danielson, *Phys. Rev.*, 1954, **93**, 46–51.
- 18 H. Kakiuchida, P. Jin and M. Tazawa, *Sol. Energy Mater. Sol. Cells*, 2008, **92**, 1279–1284.
- 19 K. Purvis, G. Lu, J. Schwartz and S. Bernasek, *J. Am. Chem. Soc.*, 2000, **122**, 1808–1809.
- 20 O. N. Mryasov and A. Freeman, *Phys. Rev. B: Condens. Matter Mater. Phys.*, 2001, **64**, 233111–233113.
- 21 A. Hjortsberg, I. Hamberg and C. Granqvist, *Thin Solid Films*, 1982, **90**, 323–326.